Jurnal Pendidikan Geografi:
Kajian, Teori, dan Praktik dalam Bidang Pendidikan dan Ilmu Geografi, 27(2), 2022, 163-174
ISSN: 0853-9251 (Print): 2527-628X (Online)
DOI: 10.17977/um017v27i22022p163-174

Automatic Geographic Information System algorithm for temporal mangrove observation: A case study in Gopek Beach, North Banten

Della Ayu Lestari*[1], Willdan Aprizal Arifin*, Novi Sofia Fitriasari*, Taufiq Ejaz Ahmad*, Amien Rais*, Dhea Rahma Azhari*

* Universitas Pendidikan Indonesia, Jl. Dr. Setiabudi No. 229, Isola, Kec. Sukasari, Kota Bandung, Jawa Barat, 40154, Indonesia
[1]Corresponding author, Email: della.ayu@upi.edu

Paper received: 10-04-2021; revised: 27-08-2021; accepted: 13-10-2021

Abstract

Temporal observation is a series of processes started by collecting the necessary data, which is then processed, so that valid information is obtained to support the right decision. To increase the ease of data collection, an automatic algorithm is needed to increase efficiency, shorten the time, and reduce the required resources. The automatic algorithm based on the geographic information system developed in this study was applied to monitoring mangrove forests in Gopek Beach, located on the north coast of Serang, Banten. Using the cloud computing process from an automatic algorithm, the results of vegetation monitoring showed increased efficiency in time and resources. Thus, this study can be used for Geographic Information Systems learning materials in schools or universities.

Keywords: algoritma otomatis; mangrove; normalized difference vegetation index; Geographic Information System

1. Introduction

The mangrove is a seedling growing in the coastal ecosystem and carrying numerous advantages for humans and its surrounding (Takarendehang et al., 2018). Meanwhile, a mangrove forest is a vegetation community consisting of various plants with dominating groups of mangroves. A mangrove forest is an ecosystem that supplies the needs of other organisms, such as birds, ocean organisms, and invertebrates (Nybakken, 2001).

Mangroves inhabit the coastal ecosystems ranging from the open sea to the estuary, which has a relatively quiet tempo of tides and waves. Mangroves can survive in an ecosystem that upholds its needs with a tolerable change of ecosystem (Purba, Kesumawati, Rambe, Zuliani, & Parinduri, 2020). The mangrove deterioration can be induced by intolerable ecosystem alteration, destroying their survivability (Barnuevo & Asaeda, 2018).

In addition, the vegetation index is an indicator explaining the green level, relative density, and vegetation health level in each of its pixels (Swets, Reed, Rowland, & Marko, 1999). Meanwhile, a different mangrove area indicates positive and negative growth of mangrove forest, with remote sensing has been used for a long time. Recent studies have discovered that remote sensing offers high accuracy in monitoring the mangrove, as well as their vegetation capacity in reflecting the type of wavelength adapted to the band from the satellite recording

provider (Akbar et al., 2020; Sohail, Khan, & Arsalan, 2020; Susantoro, Wikantika, Yayusman, Tan, & Ghozali, 2020).

The healthy and unhealthy vegetation is signified by the value of NDVI, ranging from -1 to 1. Within this common range, the negative values are attained from the non-vegetation land (ice surface and water), while the positive value is obtained from vegetated land (Sohail et al., 2020). Additionally, vegetation health can be specifically indicated in the range of 0.1–1 (Swets et al., 1999). Categorically, the healthy vegetation has NDVI values ranging from 0.3 to 1 (Gandhi, Parthiban, Thummalu, & Christy, 2015), requiring that the observed vegetation cover the same land area with a spatial resolution (Swets et al., 1999). The image that is frequently used in index value normalization is Landsat 8 with 30 meters spatial resolution and Sentinel 2 with 10 meters spatial resolution. With that resolution, the pixel in each available band represents the average value from numerous objects on the earth that reflect specific light waves divided into different bands (Fisher, Acosta, Dennedy-Frank, Kroeger, & Boucher, 2018; Shermeyer & Van Etten, 2019). In the mangrove monitoring using this index normalization calculation, each pixel in Landsat 8 with 30 meters resolution shows the average representation value from detailed vegetation in the observed area. Figure 1 illustrates the living plants in the coastal ecosystem that carry benefits for humans and their surrounding area.

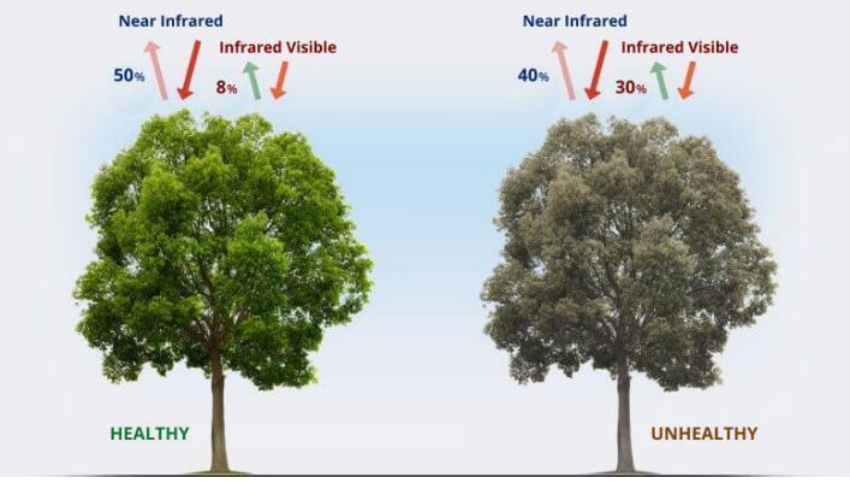

Figure 1. Comparison of *Near Infra-Red* (NIR) and Red Band (RED) Light Wave Reflection

In addition, manual data collection and data processing in mangrove monitoring have deficiencies, such as manually selecting time and cloud characteristics, as well as the ineffective offline computation that requires much time and sources (Tamiminia et al., 2020). Therefore, automation in the algorithm of Geography System Information (SIG) through cloud computing offers a solution to enhance the efficiency, required time, and sources in the spatial data extraction process (Ahmad, Cahya, & Lestari, 2020). This present study focuses on constructing and using an algorithm that facilitates a series of automatic vegetation activities monitoring, including automatic sorting and selection, automatic cloud masking, algorithm for NDVI operation, and automatic visualization of NVDI value in the form of a graph.

2. Method

This study used cloud computing to construct an algorithm for a series of automatic operations, along with Google Erath Engine, that allowed efficient and uncomplicated data

access without downloading process (Gorelick et al., 2017). The automation process was constructed based on Normalized Difference Vegetation Index (NDVI) algorithm (Deus & Gloaguen, 2013) with Formula 1.

$$\text{NDVI} = \frac{\text{NIR}-\text{RED}}{\text{NIR}+\text{RED}} \quad (1)$$

NIR : Near Infrared Band
RED : RED Band

The obtained values ranging between -1.0–1.0, representing the vegetation density, with following categorization:

< 0.1	: no vegetation
0.1–0.3	: low density
0.3–0.6	: medium density
> 0.6	: high density

Following the above categorization, a higher NDVI value represented a better density of the observed vegetation area. A sequence of the algorithm was developed with an adjustable parameter based on the user's needs to realize automatic processes of data collection to NDVI value determination.

Within this automatic algorithm, users could use three parameters, namely satellite image, observation time, and percentage of cloud cover. The satellite image from Landsat and Sentinel 2 were commonly used due to their easily understood band combination (Zhu, 2019). Aside from those satellite images, other options can be used, such as Moderate Resolution Imaging Spectroradiometer (MODIS) and others. Meanwhile, the observation time was the time required for the examination process. Notably, this observation time should be adjusted to the data available in the satellite image provider. For instance, Landsat 8 has a lower operational period in the past time than Landsat 7. It signifies that for temporal observation in the past, a combination of Landsat 8 and Landsat 7 could be used, but Landsat 7 had issues with its Scan Line Corrector causing image duplication in particular points (Miao, Zhou, Huang, Zhang, & Zhou, 2019). Thus, users had to adopt a particular method to use Landsat 7 (Sadiq, Edwar, & Sulong, 2017).

Lastly, the cloud cover percentage is a percentage from the comparison between the cloud area toward the mainland. In the NDVI calculation, the cloud carries an essential role as it may affect the error in the calculation (Aredehey, Mezgebu, & Girma, 2018). Besides, even with actual high vegetation density, if the observed area were covered with cloud, the obtained NDVI value in this algorithm would be negative (Chakraborty, Seshasai, Reddy, & Dadhwal, 2018). Additionally, the relatively visible cloud with > 50% in each pixel would be erased. After the users input those three parameters, the algorithm would automatically sort the removed smallest cloud percentage (masking) and select the lowest cloud percentage suitable for the selected time and selected image provider. Figure 2 shows the working procedures of the automatic algorithm in monitoring the mangrove density through some procedures based on the user's inputs (satellite image provider, time, and cloud percentage). The input parameters were used to select the proper image, enhancing the accuracy of the obtained NVDI value. All of the processes were automatic.

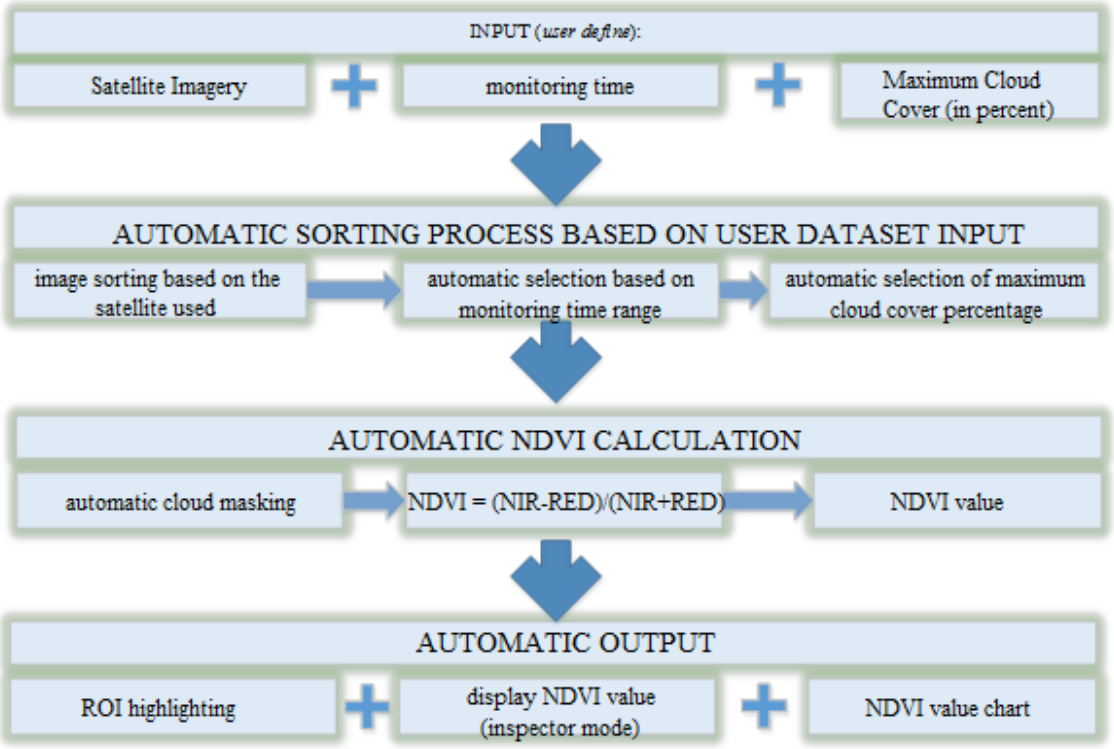

Figure 2. Automatic SIG Algorithm for Mangrove Monitoring

3. Results and Discussion

The observed areas have mangroves with developmental anomalies and homogenous vegetation with adjoining communities that are separated by the estuary. However, they have different anomaly fluctuation and trend NDVI values, as presented in Figure 3. Besides, the anomaly of changes can also be observed in the changes in the mangrove area, as shown in Table 1, as well as the time of significant emergence of the vegetation communities. Those aspects become fundamental for the grouping of the region of interest (Figure 4).

Table 1 shows the data on mangrove areas between 2014 to 2020. However, the 0 values indicate the signs of no restoration observed from NDVI values visualization or the area transformation.

Table 1. Changes in Mangrove Areas in Each Observation Areas

Year	ROI			
	A	B	C	D
2014	0	0	7650,27	71126,892
2015	0	0	7650,27	102720
2016	0	0	5911,52	115279
2017	2700	9234,94	0	125696
2018	900	9000	0	117249
2019	3600	12923,7	0	130053
2020	6339,92	16401,2	0	135824

In the NDVI visualization, a null value is obtained from the masking process so that the base map emerges from the NDVI visualization. It is due to the automatic masking occurring in the cloud value higher than 50% in each pixel. The automatic masking process aims to reduce

errors in NDVI calculation. Clouds can produce negative NDVI calculation, in which negative values should be generated from an area covered by ice and snow.

Using the automatic algorithm on Google Earth Engine, from 2014-01-01 to 2020-12-31, the obtained temporal observation results were compared with the mangrove condition in 2020 in the same location. The results are illustrated in line graph, the X-axis indicating NDVI values, Y-axis indicating observation year, and the alphabets indicate observation areas (Figure 3).

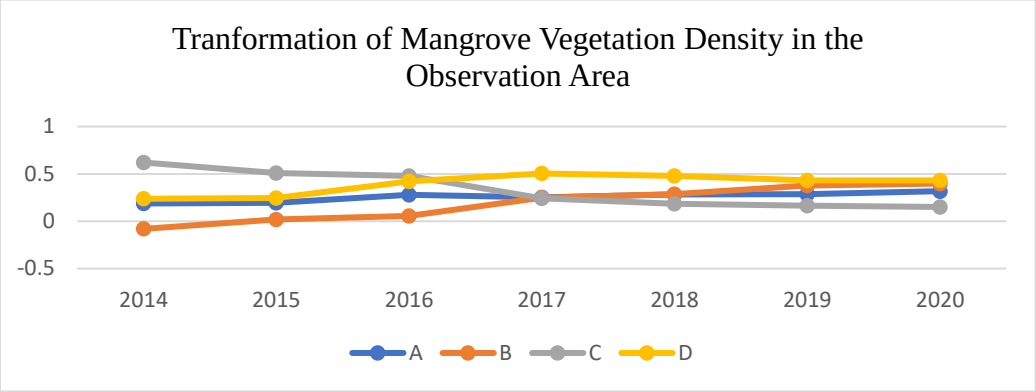

Figure 3. Visualization of Average NDVI Values from Each Observed Area

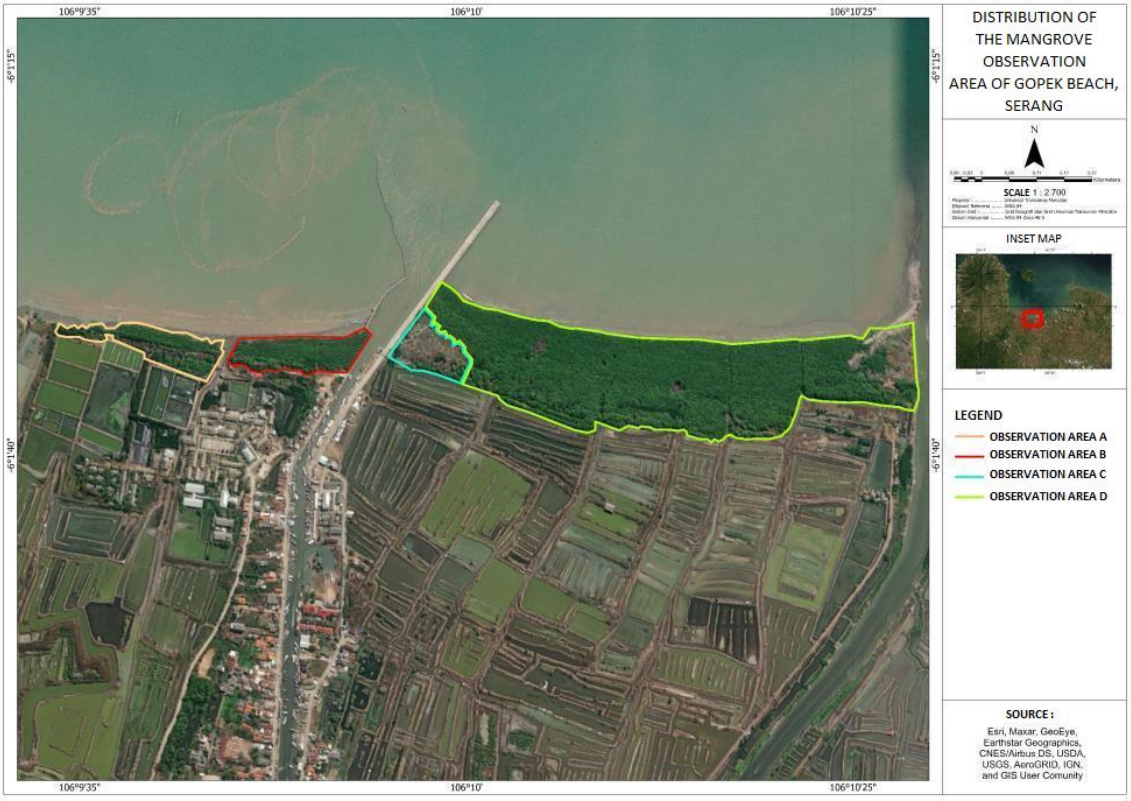

Figure 4. Mangrove Observation Area

Different mangrove vegetation densities were obtained, with a significant increase and decrease in NDVI values in specific mangrove areas on Gopek Beach between 2014 and 2020.

In all A-D observation areas, several transformations were observed, including the reduced and upsurged average NDVI values, signifying changes in the mangrove forest's quality and quantity.

The observation results in 2014 show that the A and B areas had very low mangrove vegetation density, with average values of 0.187 and -0.081 for areas A and B, respectively. As illustrated in Figure 5, A and B observation areas are dimmer than C and D areas. C and D areas have the highest average values of 0.620 and 0.237, respectively, as shown in Figure 3. The D area had a low value due to, in 2014, some of its areas being inhibited by non-mangrove, as marked by the purple color, but it has a positive value so that it can be excluded in the calculation. However, area D has a high area of healthy mangrove of 71126.892 meter^2, while the C area only has a healthy mangrove area of 7650.27m^2 (Table 1).

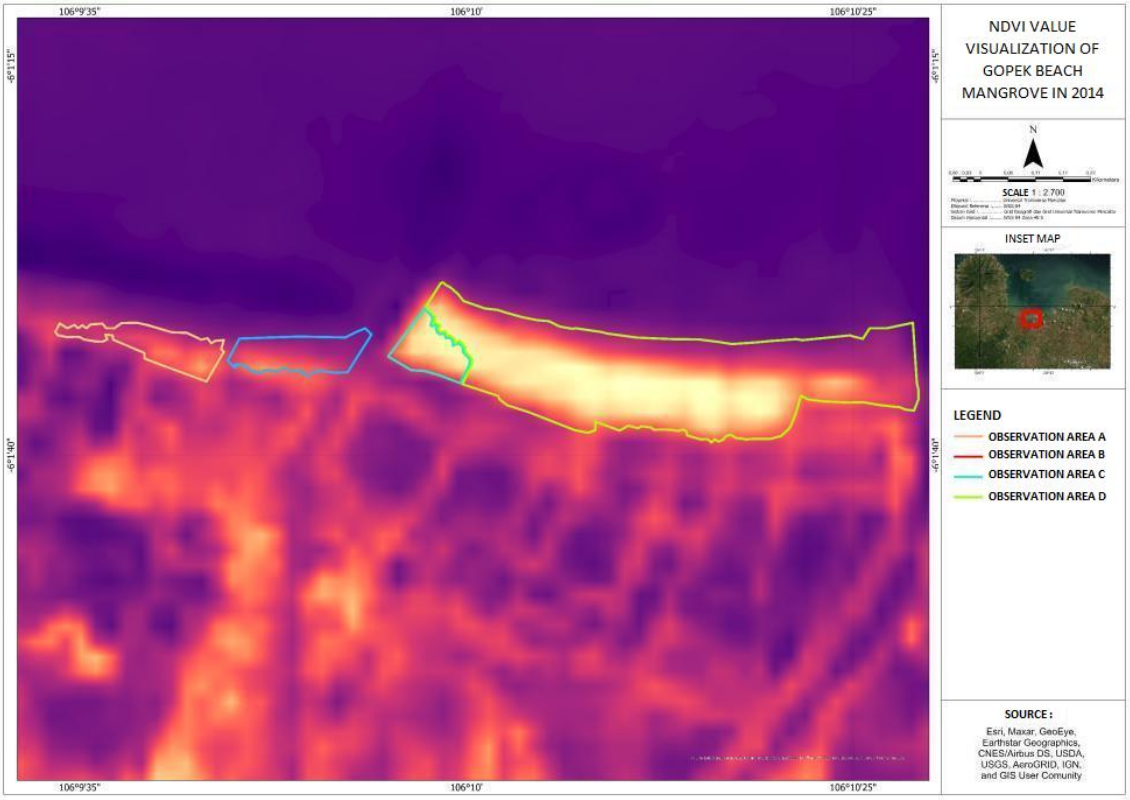

Figure 5. Mangroves' Conditions in Each Observation Area in 2014

According to Figure 6, in 2015, the observation areas A and B have a brighter color, even if they are not significant. In 2015, areas A, B, and D have increasing vegetation density to 0.194 (+0.007), 0.0173 (+0.098), and 0.245 (+0.008), respectively. Area C experiences a significant decrease of 0.508 (-0.113), while the most significant increase is observed in area B, by +0.098 (Figure 3).

In addition, area D also had positive growth with an increasing area to 102720m^2 (+31593.108 m^2), while area C remains to be 7650.27m^2 (Table 1). The findings are illustrated in the wider area with brighter colors in 2015 than in 2014.

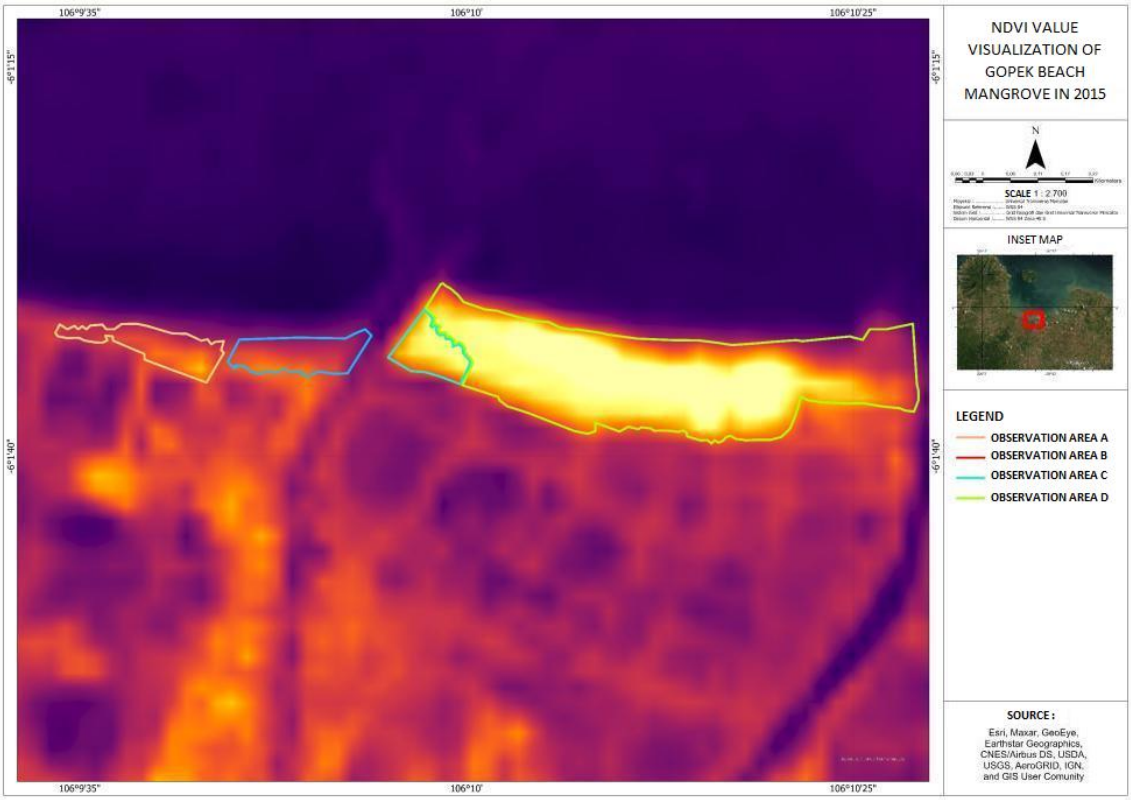

Figure 6. Mangrove Condition in Each Observation Area in 2015

The substantial differences appeared in 2016 as illustrated by different brightness, showing a more significant increase of vegetation density values in areas A, B, and D, with the average values of 0.29 (+0.085), 0.057 (+0.040), and 0.42 (+0.084), respectively. However, a decrease in vegetation density value was observed in area C, to 0.479 (-0.028) (Figure 3).

The brightness color in areas A and B (Figure 7) significantly increase from the previous years. It indicates an increase in NDVI values. Additionally, throughout 2016, area C decreased into 5911.52m^2 (-1738.75m^2), while area D increased into 115279m^2 (+12559m^2) (Table 1).

As illustrated in Figure 8, during 2017, a significant decrease in vegetation density was observed in the C area, shown by drastically darkened pixel color. It signifies a decreasing NDVI value to 0.243 (-0.237). The decrease is also observed in Are A, to 0.254 (-0.025). A significant escalation of NDVI occurred in observation areas B and D, with NDVI values of 0.247 (+0.189) and 0.504 (+0.084), respectively (Figure 3).

The results from 2017 indicate a change in the healthy mangrove area, with the most drastic decrease observed in area C. Besides, from the color changes indicator, area C had significantly reduced the healthy mangrove area to 0m^2 (-5911.52m^2). Meanwhile, the increase is observed in other areas. Area A values increase to >0.3, being the first area with that average value. Areas A, B, and D also have increasing areas of 2700m^2, 9234.94m^2, and 125696m^2 (+10417m^2), respectively.

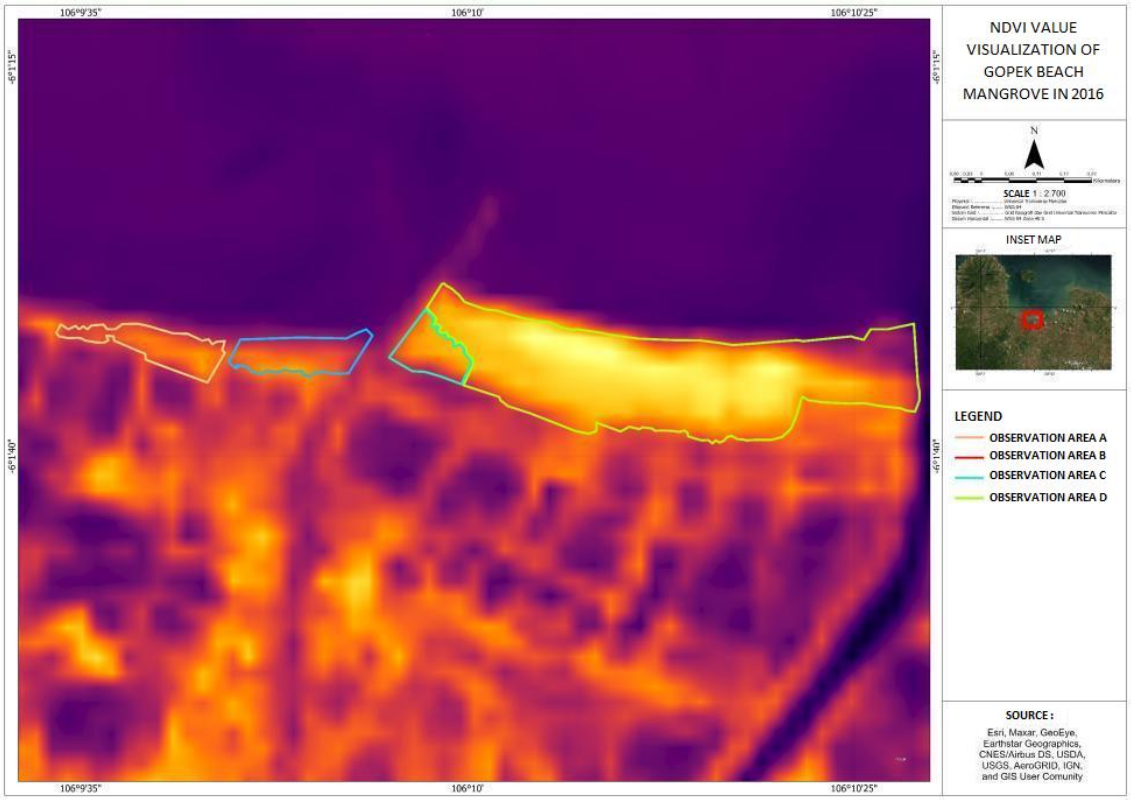

Figure 7. Mangrove Condition in Each Observation Area in 2016

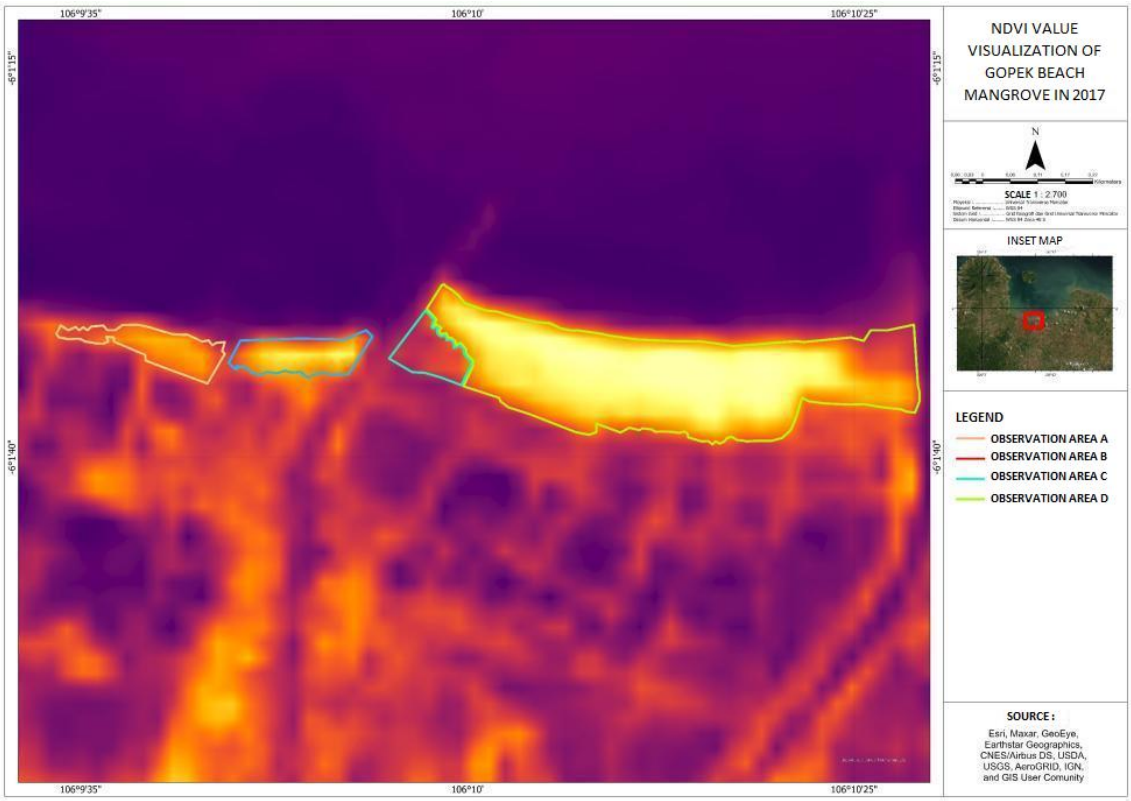

Figure 8. Mangrove Condition on Each Observation Area in 2017

Throughout 2017, areas B and D had increasing vegetation density. Meanwhile, in 2018, reduced density was observed in areas C and D, to 0.184 (-0.059) and 0.479 (-0.025). In the same year, A and B areas have a positive development relevant to the increase of vegetation density, to 0.283 (+0.029) and 0.287 (+0.039), respectively (Figure 3). From the color of the pixel, areas A and B had brighter colors, even if they were not significant (Figure 9). Additionally, the increase in healthy mangrove areas was also observed in areas A, B, and D, as shown in Table 1. Areas A, B, and D have healthy mangrove areas of 900m^2 (-1800m^2), 9000m^2 (-234.94m^2), and 117249m^2 (-8,447m^2), respectively.

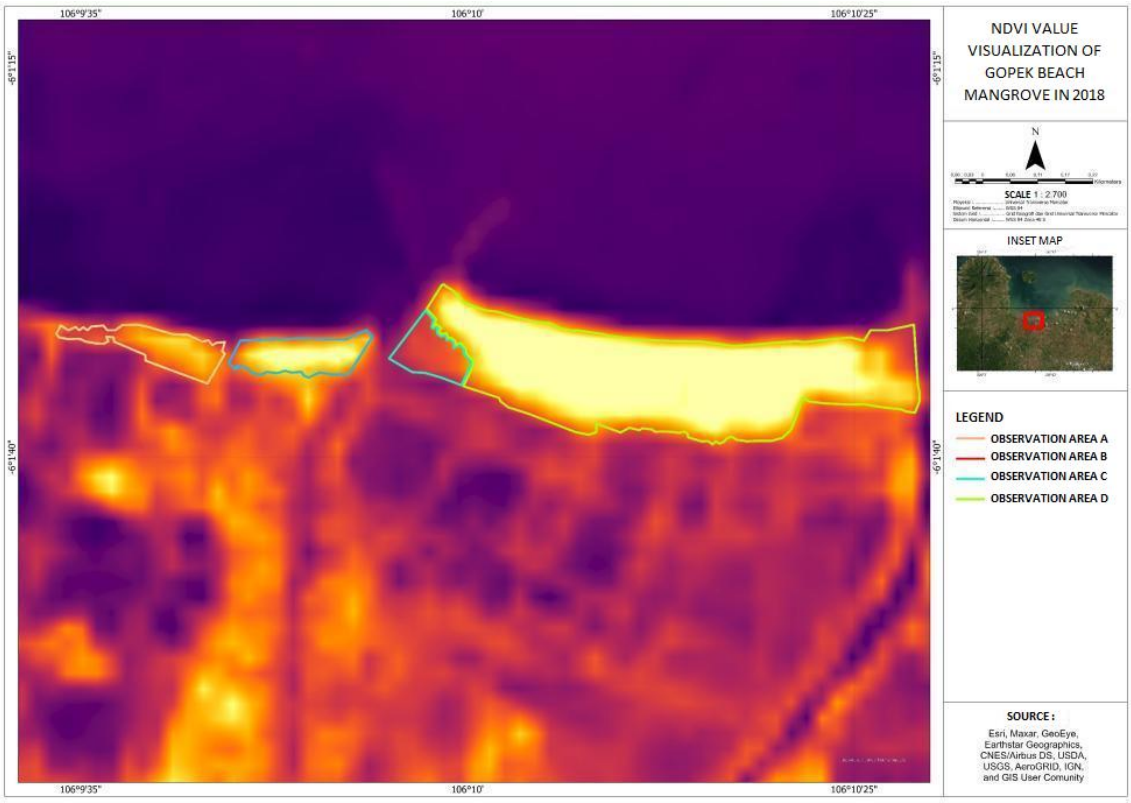

Figure 9. Mangrove Condition in Each Observation Area in 2018

In 2019, the NDVI values of areas A and B increased to 0.285 (+0.002) and 0.378 (+0.091), respectively. Meanwhile, in areas C and D, the NDVI values decreased to 0.163 (-0.020) and 0.430 (-0.049) (Figure 3). The decreases are indicated by the darkened colors of some pixels, as shown in Figure 10. The healthy mangrove area in observed areas A, B, and D increases to 3600m^2 (+2700m^2), 12923.7m^2 (+3923.7m^2), and 130053m^2 (+12804m^2) in 2019.

The results of the last observation in 2020 showed that all areas experienced an increase, except area C, as illustrated in Figure 11. The vegetation density in areas A, B, and D became 0.318 (+0.033), 0.398 (+0.020), and 0.430 (+0.0004), respectively. Besides, areas A, B, and D areas also significantly increased into 6339.92m^2 (+2739.92m^2), 16401,2m^2 (+3477.5m^2), and 135824m^2 (+5771m^2), respectively.

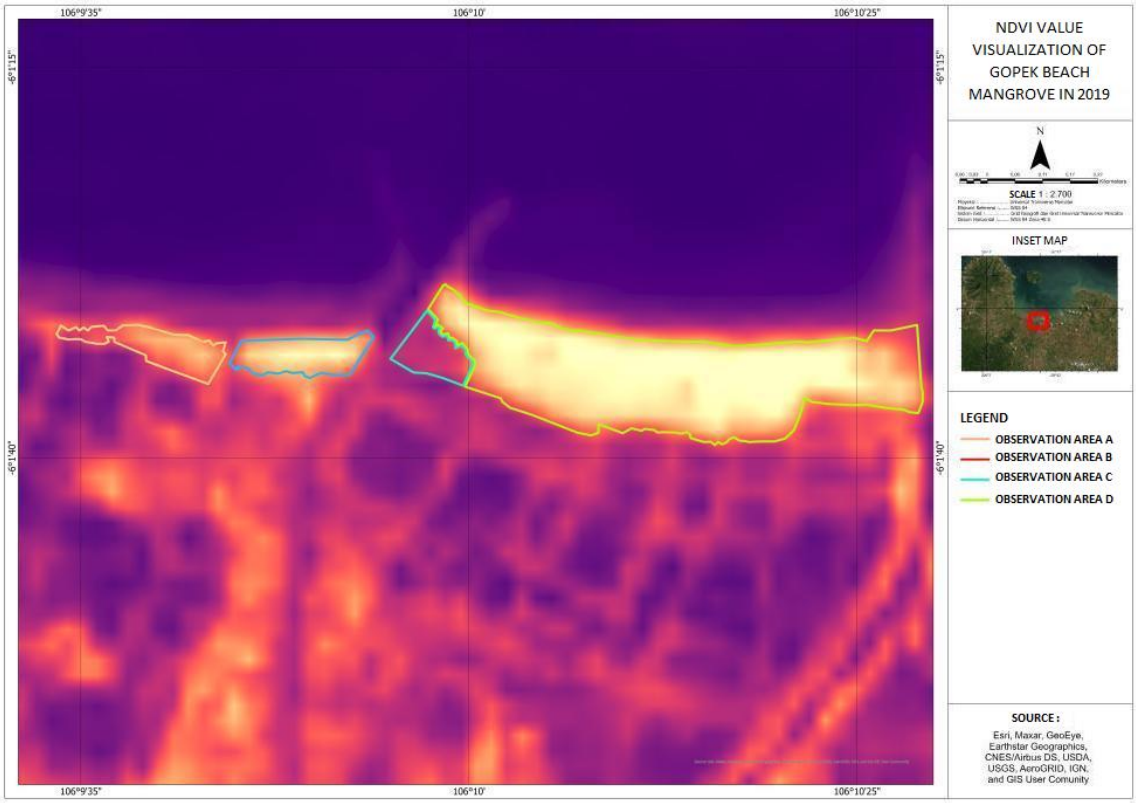

Figure 10. Mangrove Condition in Each Observation Area in 2019

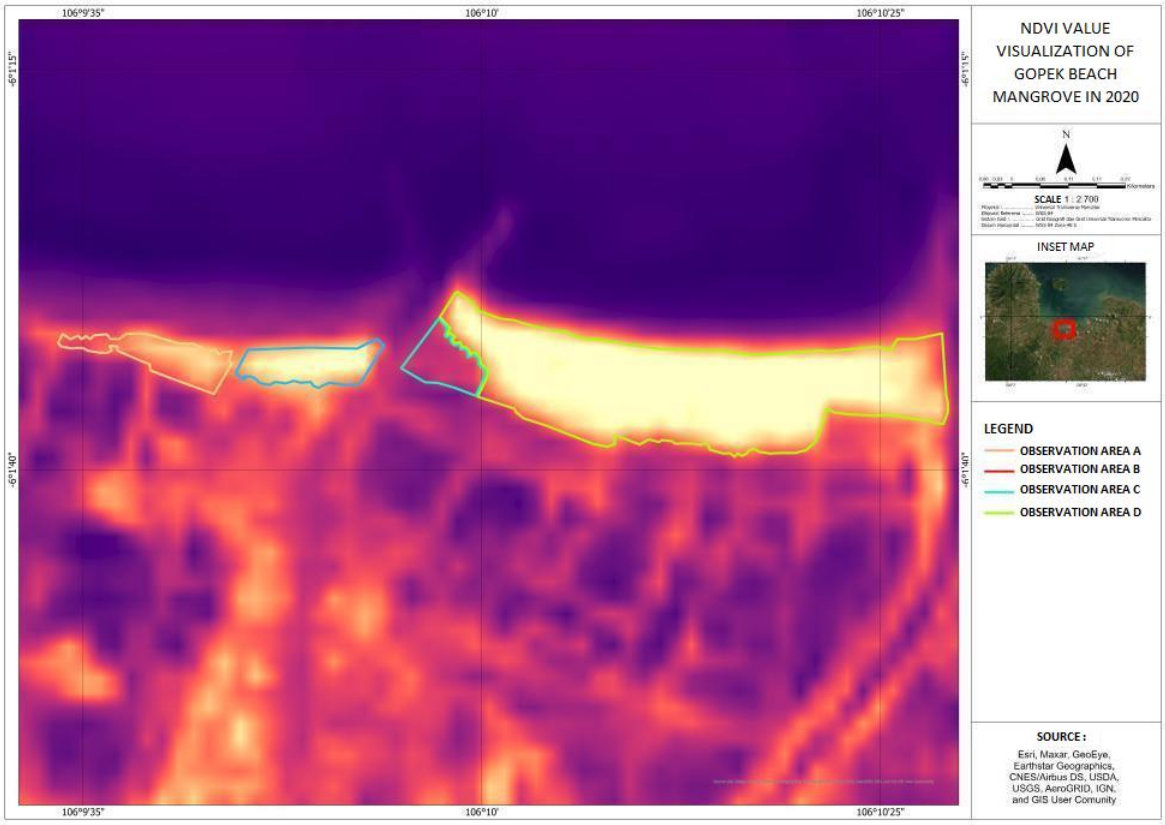

Figure 11. Mangrove Condition in Each Observation Area in 2020

This study requires further study on the factors affecting the mangrove vegetation density growth, both negatively and positively. However, area C has the most severe damage, as shown in Figure 12.

Figure 12. Compilation of Observation Photos with the Highest Severity, Showing Scattered Trash and Dead Mangrove

Figure 12 shows a board with a statement from the local officials stating that the mangrove damages were induced by an oil refinery leak on 12 July 2019. However, the results of automatic temporal observation show that the damage had occurred since 2015, with a high decrease in vegetation density.

4. Conclusion

This automatic algorithm offers numerous benefits, as proven in this study that the algorithm can strengthen our decision by confirming that the fluctuation led to mangrove death before the oil leak. As decision support, each process and output should be followed by field observation, with a table of healthy mangrove areas in each pixel algorithm to find the anomaly points, indicated by the opposite trend between the NDVI fluctuation and healthy mangrove area fluctuation. Besides, the automatic SIG algorithm has high dependability on satellite images which can be disturbed by the clouds. Thus, this automatic algorithm is highly essential for SIG learning. This automatic SIG algorithm supports Geography learning, primarily in the analysis method of mangrove temporal observation in SIG lecture.

References

Ahmad, T. E., Cahya, G. R. D., & Lestari, D. A. (2020). Penggunaan sistem informasi geografi untuk mencari lokasi yang tepat sebagai penyimpanan energi hydro terpompa. *Jurnal Georafflesia: Artikel Ilmiah Pendidikan Geografi*, *5*, 68–79.

Akbar, M. R., Arisanto, P. A. A., Sukirno, B. A., Merdeka, P. H., Priadhi, M. M., & Zallesa, S. (2020). Mangrove vegetation health index analysis by implementing NDVI (normalized difference vegetation index) classification method on sentinel-2 image data case study: Segara Anakan, Kabupaten Cilacap. *IOP Conference Series: Earth and Environmental Science*, *584*(1), 12069. IOP Publishing.

Aredehey, G., Mezgebu, A., & Girma, A. (2018). Land-use land-cover classification analysis of Giba catchment using hyper temporal MODIS NDVI satellite images. *International Journal of Remote Sensing*, *39*(3), 810–821.

Barnuevo, A., & Asaeda, T. (2018). Integrating the ecophysiology and biochemical stress indicators into the paradigm of mangrove ecology and a rehabilitation blueprint. *PLoS One*, *13*(8), e0202227.

Chakraborty, A., Seshasai, M. V. R., Reddy, C. S., & Dadhwal, V. K. (2018). Persistent negative changes in seasonal greenness over different forest types of India using MODIS time series NDVI data (2001–2014). *Ecological Indicators*, *85*, 887–903.

Deus, D., & Gloaguen, R. (2013). Remote sensing analysis of lake dynamics in semi-arid regions: Implication for water resource management Lake Manyara, East African Rift, Northern Tanzania. *Water*, *5*(2), 698–727.

Fisher, J. R. B., Acosta, E. A., Dennedy-Frank, P. J., Kroeger, T., & Boucher, T. M. (2018). Impact of satellite imagery spatial resolution on land use classification accuracy and modeled water quality. *Remote Sensing in Ecology and Conservation*, *4*(2), 137–149.

Gandhi, G. M., Parthiban, S., Thummalu, N., & Christy, A. (2015). Ndvi: Vegetation change detection using remote sensing and gis–A case study of Vellore District. *Procedia Computer Science*, *57*, 1199–1210.

Gorelick, N., Hancher, M., Dixon, M., Ilyushchenko, S., Thau, D., & Moore, R. (2017). Google Earth Engine: Planetary-scale geospatial analysis for everyone. *Remote Sensing of Environment*, *202*, 18–27.

Miao, J., Zhou, X., Huang, T. Z., Zhang, T., & Zhou, Z. (2019). A novel inpainting algorithm for recovering Landsat-7 ETM+ SLC-OFF images based on the low-rank approximate regularization method of dictionary learning with nonlocal and nonconvex models. *IEEE Transactions on Geoscience and Remote Sensing*, *57*(9), 6741–6754.

Nybakken, J. W. (2001). *Marine biology: an ecological approach* (Vol. 5). Benjamin Cummings San Francisco.

Purba, A., Kesumawati, D., Rambe, T. R., Zuliani, U. S., & Parinduri, W. M. (2020). Pengelolaan ekosistem hutan mangrove dengan memperhatikan kualitas air ditinjau dari sifat kimia di Desa Jaring Halus Langkat. *Jurnal Pengabdian Kepada Masyarakat*, *1*(2), 54–59.

Sadiq, A., Edwar, L., & Sulong, G. (2017). Recovering the large gaps in Landsat 7 SLC-off imagery using weighted multiple linear regression (WMLR). *Arabian Journal of Geosciences*, *10*(18), 1–14.

Shermeyer, J., & Van Etten, A. (2019). The effects of super-resolution on object detection performance in satellite imagery. *Proceedings of the IEEE/CVF Conference on Computer Vision and Pattern Recognition Workshops*, 0.

Sohail, U., Khan, I. A., & Arsalan, M. H. (2020). Analysis the potential of vegetation indices (NDVI) for land use/cover classification in Karachi by landsat 8 data. *International Journal of Biology and Biotechnology*, *17*.

Susantoro, T. M., Wikantika, K., Yayusman, L. F., Tan, A., & Ghozali, M. F. (2020). Monitoring of mangrove growth and coastal changes on the North Coast of Brebes, Central Java, Using Landsat Data. *International Journal of Remote Sensing and Earth Sciences (IJReSES)*, *16*(2), 197–214.

Swets, D., Reed, B. C., Rowland, J., & Marko, S. E. (1999). A weighted least-squares approach to temporal NDVI smoothing. *From Image to Information: 1999 ASPRS Annual Conference*.

Takarendehang, R., Sondak, C. F. A., Kaligis, E., Kumampung, D., Manembu, I. S., & Rembet, U. N. W. J. (2018). Kondisi ekologi dan nilai manfaat hutan mangrove di Desa Lansa, Kecamatan Wori, Kabupaten Minahasa Utara. *Jurnal Pesisir Dan Laut Tropis*, *2*.

Tamiminia, H., Salehi, B., Mahdianpari, M., Quackenbush, L., Adeli, S., & Brisco, B. (2020). Google Earth Engine for geo-big data applications: A meta-analysis and systematic review. *ISPRS Journal of Photogrammetry and Remote Sensing*, *164*, 152–170.

Zhu, Z. (2019). Science of landsat analysis ready data. *Remote Sensing*, *11*(8), 2166.